Iranian Reasearch Organization for Science and Technology (IROST)

Advances in Environmental Technology 11(3) 2025, 341-356.

Advances in Environmental Technology

Journal home page: https://aet.irost.ir

# Treatment of the spent caustic wastewater using g-$C_3N_4$/$CeFeO_3$ nanocomposites in a Taylor–Couette photocatalytic reactor

**Soleiman Mosleh**[*a], **Mostafa Narimani**[b], **Atousa Daneshyar**[b]

[a] *Polymer Engineering Department, Faculty of Gas and Petroleum, Yasouj University, Gachsaran, Iran.*

[b] *Chemical Engineering Department, Islamic Azad University, Omidiyeh Branch, Omidiyeh, Iran.*

## ARTICLE INFO

*Document Type:*
Research Paper

*Article history:*
Received 04 March 2025
Received in revised form
10 April 2025
Accepted 29 April 2025

**Keywords:**
g-$C_3N_4$/$CeFeO_3$
Nanocomposites
COD Reduction
Spent Caustic Wastewater
Catalyst Recycling
Petrochemical Plants

## ABSTRACT

The discharge of spent caustic wastewater (SCW) from petrochemical plants poses a significant environmental concern due to its high Chemical Oxygen Demand (COD). This research investigates the efficacy of a photocatalytic degradation process for treating SCW. The primary objective is to achieve maximum COD reduction while carefully managing the hydrogen peroxide ($H_2O_2$) to SCW ratio and optimizing key operational parameters. To this end, g-$C_3N_4$/$CeFeO_3$ nanocomposites were synthesized as efficient photocatalysts and thoroughly characterized using XRD, FE-SEM, EDX, FT-IR, DRS, and BET techniques. Under optimized conditions—specifically a photocatalyst loading of 1.0 g/L, an $H_2O_2$/SCW ratio of 2.50 mL/L, a pH of 5.0, a reaction time of 60 minutes, and an aeration rate of 1.50 L/min—a remarkable 98% COD removal was achieved. Furthermore, catalyst recycling studies demonstrated the reusability of the g-$C_3N_4$/$CeFeO_3$ nanocomposites for at least four consecutive treatment cycles, indicating their potential for sustainable application. Recognizing the limitations of conventional reactors for scaling up photocatalytic processes, this study also proposes the integration of the developed photocatalyst with advanced reactor designs, such as Taylor-Couette reactors, to enhance mass and photon transfer. This integration represents a critical future direction for achieving industrially viable wastewater treatment solutions.

## 1. Introduction

Pollutants present in petrochemical wastewater are significant contributors to environmental contamination, necessitating their removal to ensure effective wastewater management and compliance with environmental standards [1, 2]. Furthermore, certain pollutants can induce corrosion in pipelines and process equipment [3]. In the olefin units of petrochemical industries, furnace exhaust gases contain sulfur compounds, which are separated from olefins, hydrogen, and methane in fractionation towers using caustic solutions [4]. The resulting spent caustic solution,

---

[*] Corresponding author Tel.: + 98 9175184010
E-mail: mosleh@yu.ac.ir

DOI: 10.22104/AET.2025.7458.2075

containing sulfur compounds, constitutes the unit's wastewater and requires appropriate treatment before disposal [5]. This process aims to eliminate hydrogen sulfide, but the formation of sodium sulfide, a toxic compound, is observed in the effluent. Spent caustic is recognized as a hazardous wastewater due to its high acidity and the presence of sulfide, hydrocarbon, residual free caustic, and mineral salts [6, 7]. The caustic stream must undergo treatment, as high sulfide concentrations can cause toxicity to microorganisms in biological wastewater treatment [8]. Spent caustic poses various challenges for refining, petrochemical, and gas industries. Sulfides, mercaptans, and volatile organic compounds generate offensive odors [9, 10]. Additionally, these gases and pollutants present toxicity hazards, as they can be absorbed through the skin and into the bloodstream, leading to adverse health effects [11].

Spent caustic exhibits a high Chemical Oxygen Demand (COD), a propensity for foaming, and the potential to induce detrimental or toxic effects in biological treatment units [12]. Given the wide range of hydrocarbons present in spent caustic wastewater, the selection of novel techniques such as advanced oxidation processes (AOPs), as a primary degradation method prior to biological treatment, and subsequent to physical pretreatment, can be considered logical and effective [13]. Sulfide contamination is both toxic and highly corrosive, causing damage to equipment [14]. Furthermore, its presence in wastewater can lead to the formation of insoluble metal precipitates [15]. By employing AOPs, sulfide, sulfur compounds, and hydrocarbon compounds can be oxidized and reduced to levels meeting specified standards [16].

Various methods have been developed for caustic treatment, each justified for specific types or quantities of spent caustic compared to others. Generally, all methods are designed to reduce Biological Oxygen Demand (BOD) and COD, and the neutralized substance is sent to a Wastewater Treatment Facility (WWTF) for further treatment [17]. Treatment methods can be categorized into thermal and chemical processes, each encompassing various techniques. Thermal methods include incineration and wet air oxidation (WAO), while chemical methods consist of direct chemical oxidation, deep neutralization, and separation [18-20].

Given that direct biological treatment is not feasible for certain specific wastewaters in this industry, due to their inherent nature, innovative methods such as AOPs are being explored for the remediation of these pollutants [21 ,22]. These methods rely on the generation of highly reactive species, such as hydroxyl radicals, which can rapidly oxidize a wide range of organic contaminants [23]. Among advanced oxidation processes, heterogeneous photocatalysts have demonstrated satisfactory results in the degradation of recalcitrant and toxic organic substances, producing less toxic and biologically degradable materials [24]. Spent caustic from oil and gas refineries is recognized as a hazardous stream due to its characteristic properties, including high pH (corrosivity) and toxic components such as phenol, sodium sulfide, and mercaptans [25]. Spent caustic imposes high levels of BOD and COD on natural water resources. It also contains sulfides and mercaptans, which can lead to sediment formation or metallurgical damage in refinery equipment. Consequently, it appears to have minimal potential for in-refinery reuse. Therefore, appropriate wastewater treatment methods are essential for its safe disposal. However, commercially available disposal methods are costly and environmentally unsustainable. Hence, there is a pressing need for the development of an eco-friendly and cost-effective technology in this field. AOPs represent one such technology that has emerged as an alternative solution in wastewater treatment over the past decade [26]. The fundamental mechanism of these processes involves the generation of free radicals, which induce pollutant degradation by attacking contaminant species [27]. AOPs differ from other conventional methods in that they destroy harmful compounds and pollutants, converting them into harmless substances like carbon dioxide and water, rather than concentrating them for separation or transferring them to another phase [28]. Consequently, these processes do not produce secondary pollutants, thus eliminating the need for disposal or recovery. Previous research has explored various AOPs for wastewater treatment. A slurry bubble photoreactor employing external circulation of $SnO_2$ nanoparticles was demonstrated to effectively remove chemical oxygen demand (COD) from petroleum refinery wastewater [29]. To achieve permissible COD concentrations for wider applications, an electrocoagulation reactor has been implemented to treat real oily wastewater effluent from a petroleum refinery [30]. Furthermore, the efficacy of electrocoagulation in the removal of COD, biochemical oxygen demand (BOD), oil & grease, and turbidity from oil-field produced water has been investigated [31]. Comparative analyses of mesoporous $TiO_2$ nanoparticles and commercial $TiO_2$ photocatalysts have been conducted in the context of phenol photodegradation and COD reduction in industrial wastewater derived from the pharmaceutical sector [32]. Additionally, the photocatalytic degradation process has been evaluated for its capacity to remove turbidity and COD from municipal wastewater [33].

The use of photocatalytic materials for pollutant degradation is one method within the realm of AOPs. The photocatalytic process essentially enhances light-induced reactions in the presence of a catalyst. Upon illumination, photocatalysts are activated and generate free radicals with high oxidizing power, leading to the degradation of various organic and inorganic materials. In this research, the degradation process of spent caustic is investigated through the design of a photocatalytic reactor and the synthesis of an efficient photocatalyst. Metal-free polymeric graphitic carbon nitride (g-$C_3N_4$) stands out as an efficient and robust visible-light-driven photocatalyst [34]. However, its practical application has been limited by its small specific surface area, rapid recombination of photogenerated electron-hole pairs, and the difficulty in recycling its powdered form from aqueous solutions, leading to catalyst loss [35]. Therefore, developing an efficient and reusable g-$C_3N_4$-based photocatalyst for contaminant degradation is crucial [36]. One way to overcome the limitations of this catalyst is by fabricating composites with other structures, including metal oxides, nanostructures, and Metal-Organic Frameworks (MOFs). Among different materials, Iron-based MOFs (Fe-MOFs) have garnered significant interest due to their inherent porosity and semiconductor properties [37]. The presence of Fe-oxygen clusters, which exhibit strong absorption in the visible light spectrum, further positions Fe-MOFs as promising materials for photocatalysis [38]. Consequently, integrating Fe-MOFs with g-$C_3N_4$ has emerged as a strategy to enhance photocatalytic efficiency. Notably, the intimate combination of g-$C_3N_4$ with Mn–Fe bimetallic nanostructures can yield electrocatalysts with highly conductive skeletons, metal-based core-shell structures, and uniquely intertwined, hierarchically porous architectures. These exceptional characteristics are advantageous for exposing ample active sites, modifying the electronic structure, and facilitating interfacial charge transfer. Furthermore, they strengthen the interfacial contact between metal-based nanoparticles and the graphitic carbon shell, ultimately ensuring high catalytic activity and stability for reactions such as oxygen reduction. This approach of combining g-$C_3N_4$ with Fe-based or bimetallic Mn-Fe MOFs holds significant promise for creating improved photocatalytic and electrocatalytic materials [39]. Hence, in this research, g-$C_3N_4$/$CeFeO_3$ nanocomposites was initially synthesized for activity under visible light, and its structure was subsequently characterized using various methods, including XRD, FE-SEM, EDX, FT-IR, DRS, and BET. The photocatalyst's ability to function within the visible light range for the degradation process was then evaluated.

Another innovation of this work is the design of an efficient photocatalytic reactor, termed a Taylor-Couette reactor, to overcome external mass transfer limitations. One of the limitations in photocatalytic degradation processes that hinders scale-up is the lack of an optimal and efficient reactor. Conventional reactors typically suffer from mass transfer and photon transfer limitations, necessitating the design of a novel reactor to overcome these limitations. Taylor-Couette reactors represent a promising technology for the intensification of processes limited by mass transfer phenomena [40]. This is attributed to their inherent capacity to precisely modulate shear stresses and residence time distributions, facilitate homogeneous mixing, and provide elevated surface area-to-volume ratios [41]. A Taylor-Couette reactor is fundamentally constructed as a cylindrical vessel housing a coaxially inserted inner cylinder, thereby defining an annular space. While both cylindrical surfaces can be rotated at defined angular velocities, the outer cylinder is typically held stationary in the majority of applications [42]. The hydrodynamic conditions within the reactor, specifically the mixing characteristics, are established independently of axial flow through the manipulation of the cylinders' rotational speed and key dimensionless parameters, including the aspect ratio, the ratio of the inner to outer cylinder diameters, and the radial gap width [43]. The vortical structures generated within Taylor-Couette reactors exhibit the potential to induce efficient radial and axial convective transport [44]. Furthermore, the thickness of the fluid boundary layer between the fluid and the light source is minimized, resulting in optimal light exposure times and uniform radiation intensities [45]. In summary, the utilization of this reactor results in an enhanced mass transfer rate and photon transfer rate.

The novelty of this research lies in the synergistic combination of a novel photocatalyst (g-$C_3N_4$/$CeFeO_3$ nanocomposite) and an efficient reactor design (Taylor-Couette reactor) to address the limitations of conventional spent caustic treatment methods. While g-$C_3N_4$ shows promise as a metal-free photocatalyst, its practical use is hindered by factors like low surface area and difficulty in recovery. This study aims to overcome these limitations by synthesizing a composite with $CeFeO_3$, an iron-based material with visible light absorption properties, to enhance photocatalytic efficiency and potentially improve reusability. Furthermore, the introduction of a Taylor-Couette reactor is intended to mitigate external mass transfer and photon transfer limitations that typically impede the scale-up of photocatalytic degradation processes.

## 2. Materials and methods

### *2.1. Materials and reagents*

Cerium (III) nitrate hexahydrate ($Ce(NO_3)_3{\cdot}6H_2O$, 98.50%), Iron (III) nitrate nonahydrate ($Fe(NO_3)_3{\cdot}9H_2O$, 98%), Melamine ($C_3H_6N_6$, 99%), and Ethanol ($CH_3CH_2OH$, 99.90%) were purchased from Merck company. All chemical materials were of analytical grade and used without further purification. Deionized water was used in all experiment.

### *2.2. Material synthesis and characterization*

### *2.2.1. Synthesis of Graphite Carbon Nitride (g-$C_3N_4$)*

To synthesize g-$C_3N_4$, 0.50 g of melamine was initially added to a covered ceramic crucible and placed in a muffle furnace. It was then heated to 550 °C with a gradual ramp rate (20 °C/min) and maintained at this temperature for 2 hours. Subsequently, the ceramic crucible was removed from the furnace to allow the resulting product to cool to ambient temperature and then ground into a powder.

### *2.2.2. Synthesis of $CeFeO_3$/g-$C_3N_4$ Nanocomposites*

Initially, 0.604 g of $Ce(NO_3)_3{\cdot}6H_2O$ and 0.562 g of $Fe(NO_3)_3{\cdot}9H_2O$ were dissolved in 10 mL of deionized water and stirred at ambient temperature for 60 minutes. Subsequently, both solutions were mixed and stirred vigorously for another 60 minutes. Then, 0.50 g of g-$C_3N_4$ was added to the mixture and stirred for an additional 60 minutes. The resulting suspension was then placed in an oven at 80 °C for 12 hours to dry. Following this, the precipitate was collected and centrifuged (10,000 rpm, 20 minutes), and after multiple washes with water and ethanol, dried in an oven at 65 °C for 12 hours. Finally, the obtained product was calcined at 400 °C for 2 hours in a furnace.

### *2.2.3. Characterization*

All pH measurements were performed using a Metrohm Model-692 pH/Ion Meter. A RH basic2 IKA (Germany) heating stirrer, a Sartorius BP110S (Germany) four-digit digital balance with an accuracy of ±0.0001 g, a Griffin (UK) muffle furnace and oven, and a Sigma 16P (Germany) centrifuge were utilized. Temperature regulation and stabilization were achieved using a bath equipped with a temperature control and water circulation system. X-ray diffraction (XRD) analysis was conducted using a Philips PW-1730 (Netherlands) instrument. Field-emission scanning electron microscopy (FE-SEM) was performed using a TE-SCAN Mira III (Czech Republic) microscope. Fourier-transform infrared spectroscopy (FT-IR) was carried out using a Thermo AVATAR (USA) spectrometer. Brunauer-Emmett-Teller (BET) surface area and porosity analysis were performed using nitrogen gas with a BEL BELSORP MINI II (Japan) instrument. Diffuse reflectance spectroscopy (DRS) was measured using an Avantes Avaspec-2048-TEC spectrometer with an AvaLamp DH-S setup. Ultraviolet-visible spectrophotometry calculations were performed using a Shimadzu UV-160 (Japan) instrument. COD was measured using HACH LCK 014 kits.

### *2.4. Photocatalytic Degradation Process for COD Reduction*

To evaluate the photocatalytic capabilities of $CeFeO_3/g\text{-}C_3N_4$ Nanocomposites, this photocatalyst was employed for the treatment of spent caustic wastewater (SCW). Through experimental investigation, optimal conditions were identified, resulting in maximum COD removal. Various parameters were examined in this study, including photocatalyst loading (g/L), $H_2O_2$/SCW ratio (mL/L), pH level, reaction time (min), and aeration rate (L/min) .For conducting the experiments, a Taylor–Couette photocatalytic reactor with a total volume of 1500 $cm^3$ was utilized (Figure 1). A mechanical stirrer was incorporated to facilitate mixing within the reactor. To ensure adequate aeration of the solutions, an air pump was used to supply the necessary oxygen. Temperature was controlled by circulating cooling water through the reactor jacket .In each experiment, 1 L of solution was adjusted to the desired pH using $H_2SO_4$ and NaOH. Subsequently, this solution was introduced into the reactor. The stirrer was then activated, and a specific amount of photocatalyst was added to achieve the target concentration. To maximize the adsorption of photocatalyst particles and establish equilibrium, the stirring process continued for 30 minutes before the light source was activated. Upon activation of the light source, the aeration system was also initiated. At specific intervals (after 15, 30, 45, 60 and 75 min), 5 mL of the sample was taken from the mixture and quickly centrifuged at 10,000 rpm for 1 min. Finally, COD of the solution was determined using a COD meter at various intervals. The raw wastewater characteristics were obtained from the spent caustic neutralization section produced in the olefin unit of a petrochemical industry. These characteristics are presented in Table 1, which were used as the influent wastewater sample for the photoreactor.

## 3. Results and discussion

### *3.1. Structural and morphological characterization of samples*

Results indicate that for the $CeFeO_3$ nanoparticles (Figure 2), well-resolved XRD reflections were observed at 2θ angles of 25.35°, 32.29°, 36.8°, 39.8°, 47.7°, 55°, 57.8°, 62.8°, and 67.58°. These peaks correspond to the (111), (112), (021), (202), (221), (422), (204), (551), and (331) crystal planes of $CeFeO_3$, which can be indexed to an orthorhombic structure (ICCD: 00-022-0166). The $g\text{-}C_3N_4$ sample exhibited two diffraction peaks at 13.2° and 27.5°, corresponding to the (100) and (002) diffraction planes, respectively.

The FT-IR spectrum of the $g\text{-}C_3N_4/CeFeO_3$ photocatalyst is shown in Figure 3. A strong absorption band in the range of 1200-1650 $cm^{-1}$ is attributed to the typical skeletal stretching vibration of triazine or tri-s-triazine. The peak at 1622 $cm^{-1}$ corresponds to the C-N stretching vibrational mode, while the peaks observed at 1238, 1320, and 1409 $cm^{-1}$ are associated with the C-N heterocycle stretching of $g\text{-}C_3N_4$. The sharp peak observed at 808 $cm^{-1}$ in the spectra of all $g\text{-}C_3N_4$ samples is a characteristic out-of-plane bending vibrational mode of triazine units. The absorption band observed at 857 $cm^{-1}$ is attributed to metal-oxygen stretching (Ce-O stretching). The peak at 1093 $cm^{-1}$ is due to the metal-hydroxide bond Ce-OH, and finally, the band around 937 $cm^{-1}$ is attributed to the Ce-Fe bond in cerium orthoferrite. Other existing bands can be assigned as follows: the peaks at 3453, 3424, 1643, and 1636 $cm^{-1}$ indicate the presence of adsorbed water.

**Table 1.** Main characteristics of the utilized wastewater.

| Characteristic | Measurement unit | Amount |
|---|---|---|
| COD | mg/L | 1360 |
| TDS | mg/L | 285 |
| $Na_2S$ | wt % | 0.5 |
| pH | - | 12.70 |
| $Na_2CO_3$ | wt % | 2.5 |
| NaOH | wt % | 3 |
| Phenols | mg/L | 420 |

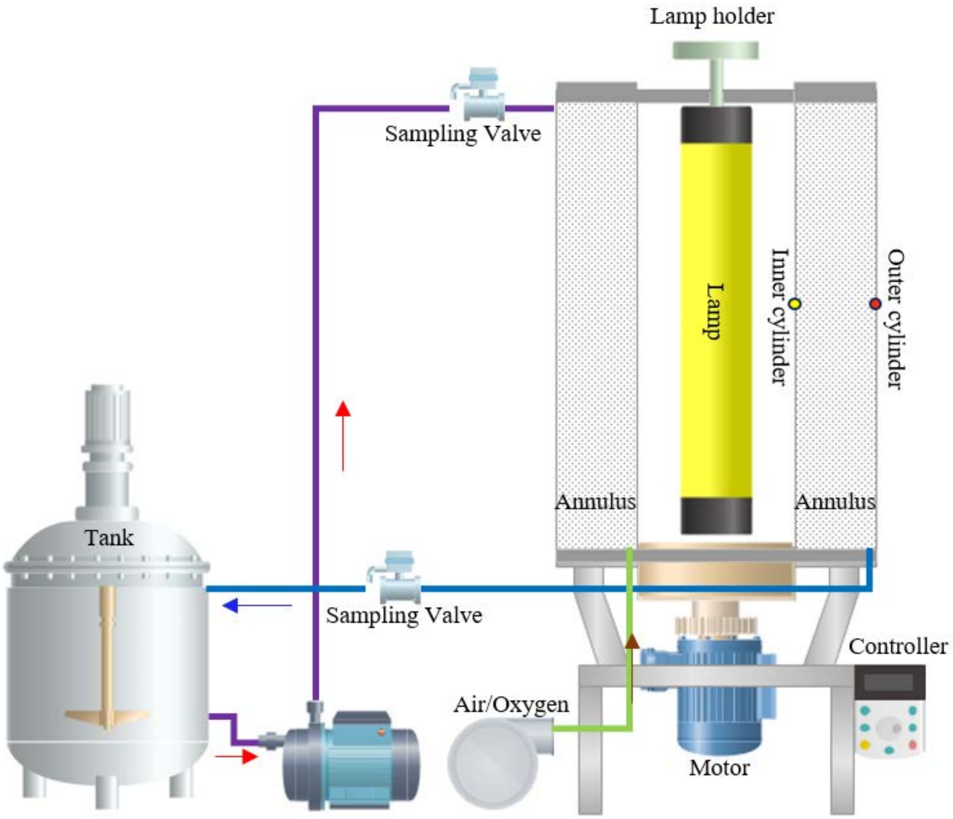

**Fig. 1.** Schematic diagram of the experimental setup.

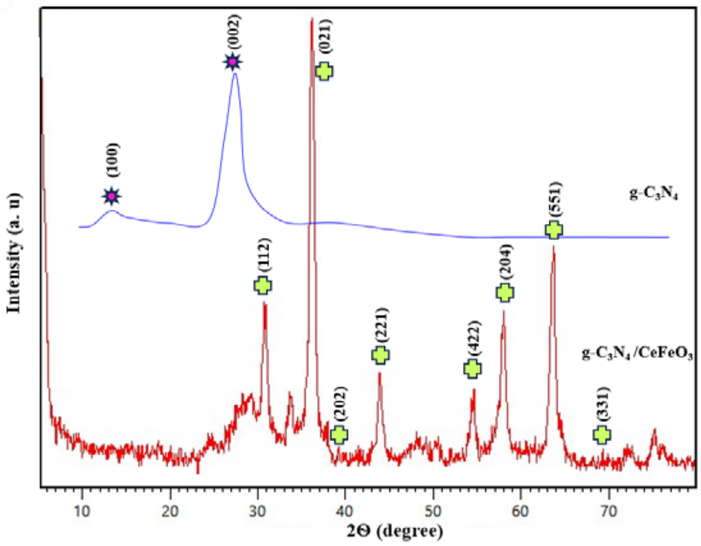

**Fig. 2.** XRD patterns of the prepared samples.

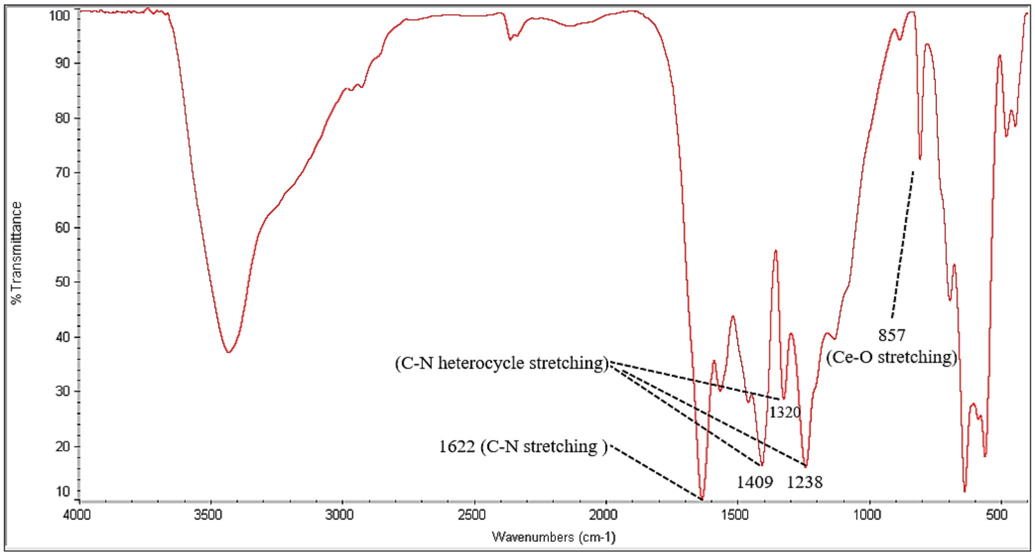

**Fig. 3.** FTIR spectrums of the g-$C_3N_4$/$CeFeO_3$ nanocomposite.

FE-SEM images (Figure 4) reveal a non-uniform distribution of shapes and strong agglomeration, which may be attributed to inherent interactions between the magnetic nanoparticles. The agglomeration of nanoparticles may arise from the thermal treatment involving elevated calcination temperatures. EDX analysis of the g-$C_3N_4$ samples coated with $CeFeO_3$ (Figure 5) revealed the presence of Ce, Fe, C, N, and O elements in the nanocomposite, confirming the phase identified by XRD analysis.

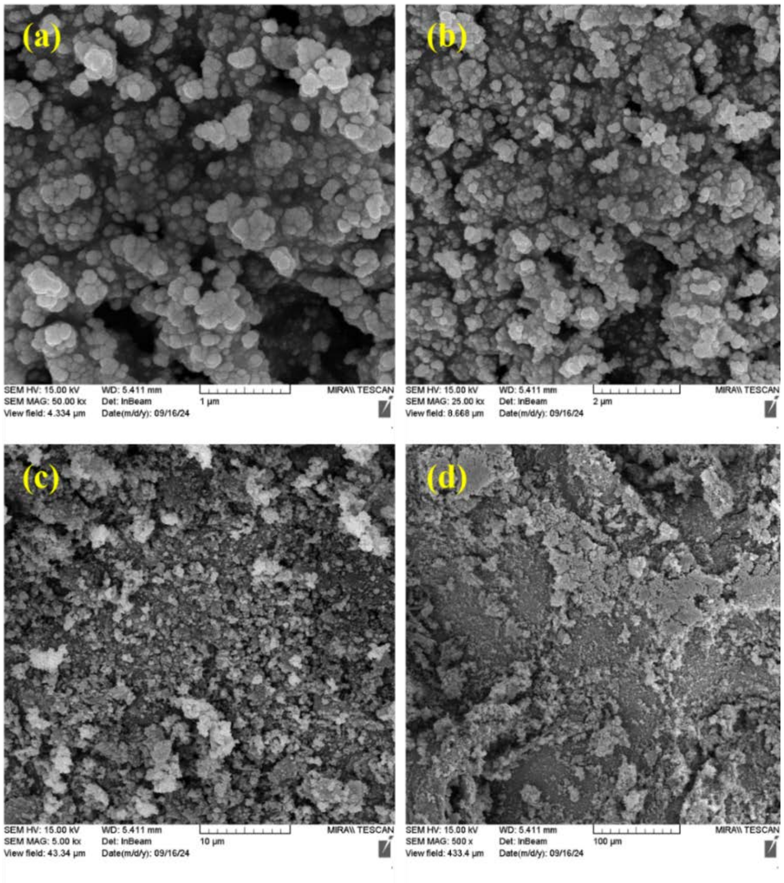

**Fig. 4.** FE-SEM images of the g-$C_3N_4$/$CeFeO_3$ nanocomposite. (a): 1 μm scale, (b): 2 μm scale, (c): 10 μm scale, and (d): 100 μm scale.

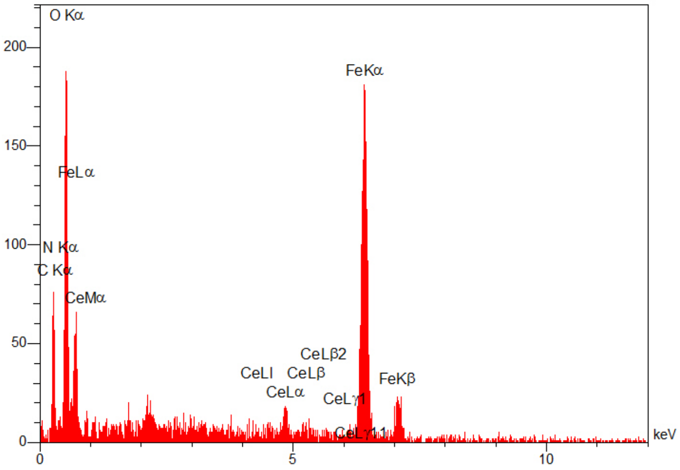

**Fig. 5.** EDX spectra of g-$C_3N_4$/$CeFeO_3$ nanocomposite.

In Figure 6, elemental mapping analysis was employed to generate visual representations of the elemental distribution within the sample, demonstrating a favorable dispersion of elements in the synthesized photocatalyst. The particle size distribution of the g-$C_3N_4$/$CeFeO_3$ photocatalyst are presented in Figure 7. Based on these images, the average particle size was determined to be in the range of 50 to 70 nm. DRS analysis was performed to understand the optical properties of the synthesized photocatalysts (Figure 8). The optical band gap energy ($E_{bg}$) of the prepared photocatalysts was calculated via Tauc plots. The $E_{bg}$ values were determined to be 1.87 eV and 2.52 eV for g-$C_3N_4$/$CeFeO_3$ NCs and g-$C_3N_4$, respectively.

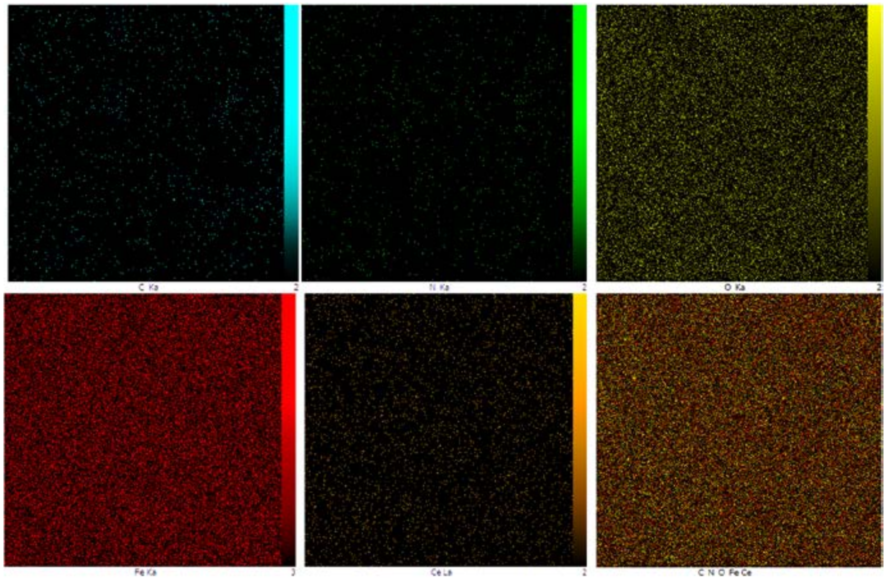

**Fig. 6.** Elemental mapping analysis of the g-$C_3N_4$/$CeFeO_3$ photocatalyst.

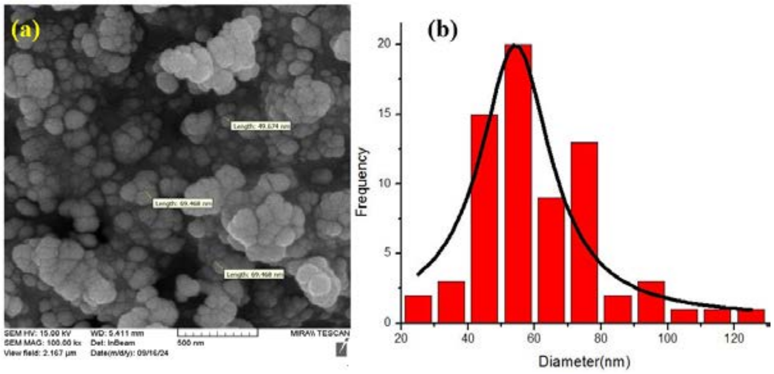

**Fig. 7.** FE-SEM image (a), and particle size distribution of the g-$C_3N_4$/$CeFeO_3$ (b).

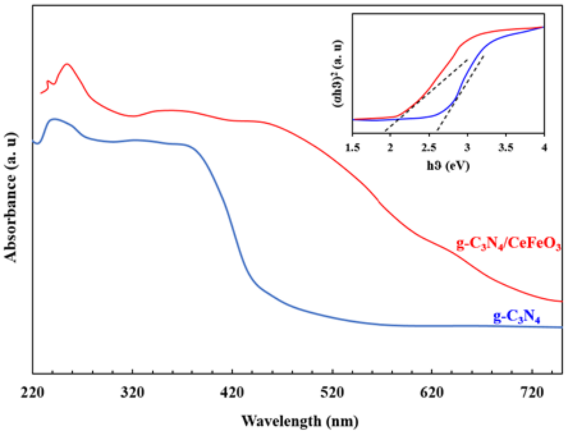

**Fig. 8.** DRS analysis for band gap measurement of the prepared samples.

The textural properties and physicochemical characteristics of the g-$C_3N_4$/$CeFeO_3$ sample, such as pore diameter (DBJH), surface area (BET), and total pore volume (Vtotal), are presented in Table 2.

**Table 2.** Data obtained by BET and BJH analyses of the g-$C_3N_4$/$CeFeO_3$ nanocomposites.

| $S_{BET}$ ($m^2$ $g^{-1}$) | $V_{total}$ ($cm^3$ $g^{-1}$) | Mean pore diameter (nm) |
|---|---|---|
| 32.10 | 0.29 | 36.98 |

Nitrogen adsorption-desorption measurements of the g-$C_3N_4$/$CeFeO_3$ photocatalyst (Figure 9) reveal a BET surface area of 32.10 $m^2$/g for the sample. The average pore diameter and high BET surface area of the synthesized sample suggest that the photocatalyst can achieve high efficiency in the degradation process.

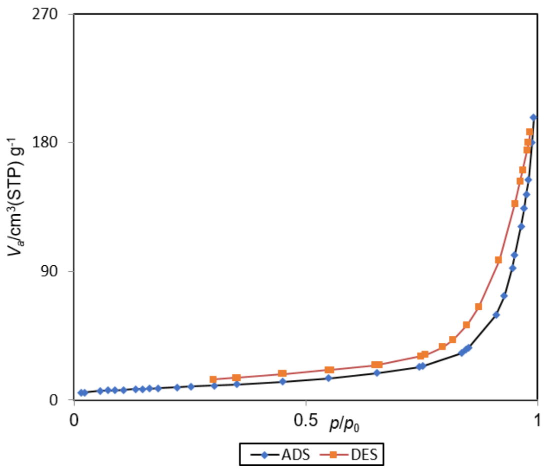

**Fig. 9.** $N_2$ adsorption-desorption isotherms of the g-$C_3N_4$/$CeFeO_3$ nanocomposites.

### *3.2. Photocatalytic performance of the g-$C_3N_4$/$CeFeO_3$ nanocomposites for COD reduction*

To evaluate the photocatalytic degradation process of g-$C_3N_4$/$CeFeO_3$ nanocomposites, this photocatalyst was utilized for the reduction of COD in discarded caustic wastewater. The influence of impactful parameters such as pH, photocatalyst loading (g/L), aeration rate (L/min), reaction time (min), and the hydrogen peroxide to caustic wastewater ratio (mL/L) on the COD reduction rate in the discarded caustic wastewater treatment process was investigated.

The effect of photocatalyst loading was also investigated. Increasing the photocatalyst concentration leads to an increase in the number of active sites on the catalyst surface. These sites act as electron-hole pair generation centers. The generated free electrons can react with molecular oxygen to produce superoxide radicals ($O^{2-}$). Conversely, positive holes can react with water molecules to generate hydroxyl radicals ($^{\bullet}OH$). Hydroxyl radicals, recognized as the strongest known oxidant, are capable of mineralizing numerous stable organic compounds. Consequently, with an increase in photocatalyst concentration and the resulting increase in free radical generation, the rate of oxidation reactions significantly increases, and the pollutant removal efficiency improves (Figure 10-a). However, exceeding an optimal photocatalyst loading threshold, identified in this study as approximately 1.05 g/L, results in a discernible decline in degradation percentage. This reduction in performance is attributed to the attenuation of light penetration depth within the reaction medium. Specifically, higher particulate concentrations lead to increased light scattering and absorption, effectively diminishing the photon flux available for photocatalyst activation. Consequently, exceeding the aforementioned threshold results in increased opacity of the suspension, creating suboptimal light conditions and a reduction in the extent of chemical oxygen demand (COD) abatement.

pH is a key parameter in photocatalytic processes. Generally, photocatalytic processes exhibit higher efficiency in acidic environments. Increasing pH at low concentrations of oxidizing agents leads to a decrease in efficiency, indicating an inverse interaction between pH and the oxidant on the process. Increasing photocatalyst concentration necessitates an increase in pH to prevent particle agglomeration. Hydroxyl radical generation primarily occurs through the positive hole reaction with water molecules or hydroxide ions. The deficiency of secondary hydroxyl radical generation sources (such as hydroperoxyl radicals) is compensated by increasing the photocatalyst loading. In alkaline environments, adsorbate adsorption on the catalyst surface decreases, subsequently reducing the degradation rate. In this study, the most effective reduction in Chemical Oxygen Demand (COD) was observed when the pH was approximately 5.0 (Figure 10-b). This is attributed to the maximized generation of hydroxyl radicals ($OH\bullet$) under these specific acidic conditions. As the pH increased beyond 5.0, a rapid conversion of $OH\bullet$ into its conjugate base, the oxide radical anion ($O\bullet-$), occurred. This anionic species exhibits a significantly lower reactivity towards organic pollutants compared to the highly potent $OH\bullet$ radical. Consequently, the overall efficiency of the COD removal process diminished with increasing pH values.

The present study demonstrates that optimizing the aeration rate can be utilized as a key parameter in the design and operation of advanced oxidation process water treatment systems. Increasing the aeration rate leads to improved mixing and consequently enhances the mass transfer of oxygen and catalyst particles. This results in an increased production of free radicals, ultimately leading to a significant reduction in COD levels in the effluent (Figure 10-c). The findings of this research can be employed in the design of higher-efficiency and lower-cost treatment systems.

The results of Figure 10-d demonstrate that increasing the irradiation time in photocatalytic processes is directly correlated with an enhancement in the removal efficiency of organic pollutants. With an increase in irradiation time, a greater number of light photons impinge upon the catalyst surface, leading to the generation of electron-hole pairs. These generated charge carriers can react with organic pollutants present in the solution and oxidize them. Furthermore, as the irradiation time increases, the probability of direct and indirect oxidation reactions increases, consequently improving the pollutant removal efficiency.

In advanced oxidation processes, hydrogen peroxide acts as a potent oxidizing agent. Increasing the hydrogen peroxide concentration augments the number of hydrogen peroxide molecules per unit volume. In the presence of light and a photocatalyst, hydrogen peroxide decomposes into hydroxyl radicals. Due to their high reactivity, hydroxyl radicals are capable of oxidizing a wide range of organic pollutants present in wastewater. With an increase in hydroxyl radical concentration, the rate of oxidation reactions accelerates, consequently reducing the COD level (Figure 10-e).

### *3.3. Process Optimization*

Optimization of operational variables in the degradation process demonstrates that the maximum treatment efficiency, achieving a 98% COD reduction, is obtained under the optimal operational variable conditions of 1.0 g/L photocatalyst loading, a pH of 5, a 2.5 mL/L hydrogen peroxide to caustic wastewater ratio ($H_2O_2$/SCW), a 60-minute operation time, and an aeration rate of 1.50 L/min.

### *3.4. Durability and Reusability of the g-$C_3N_4$/$CeFeO_3$ nanocomposites*

Catalyst stability and reusability are among the most critical factors in the economic and environmental assessment of catalytic processes. The results of this study demonstrate that the synthesized catalyst exhibits acceptable stability and can be utilized as an effective and economical catalyst for the treatment of industrial wastewater. The stability and reusability of the synthesized catalyst for the COD reduction process were investigated over four consecutive experimental cycles (Figure 11). Following each cycle, the catalyst was regenerated through washing and drying at 60 °C and subsequently reused under identical laboratory conditions. The performance of the $CeFeO_3$/g-$C_3N_4$ nanocomposites decreased by up to 6.44%, 13.72%, 21.53%, and 26.44% after one, two, three and four consecutive cycles of reuse, respectively. The results indicated that despite repeated use, the catalyst maintained acceptable stability, and its catalytic activity did not significantly diminish. Furthermore, the simple and effective regeneration method employed in this study played a crucial role in preserving the catalyst's activity.

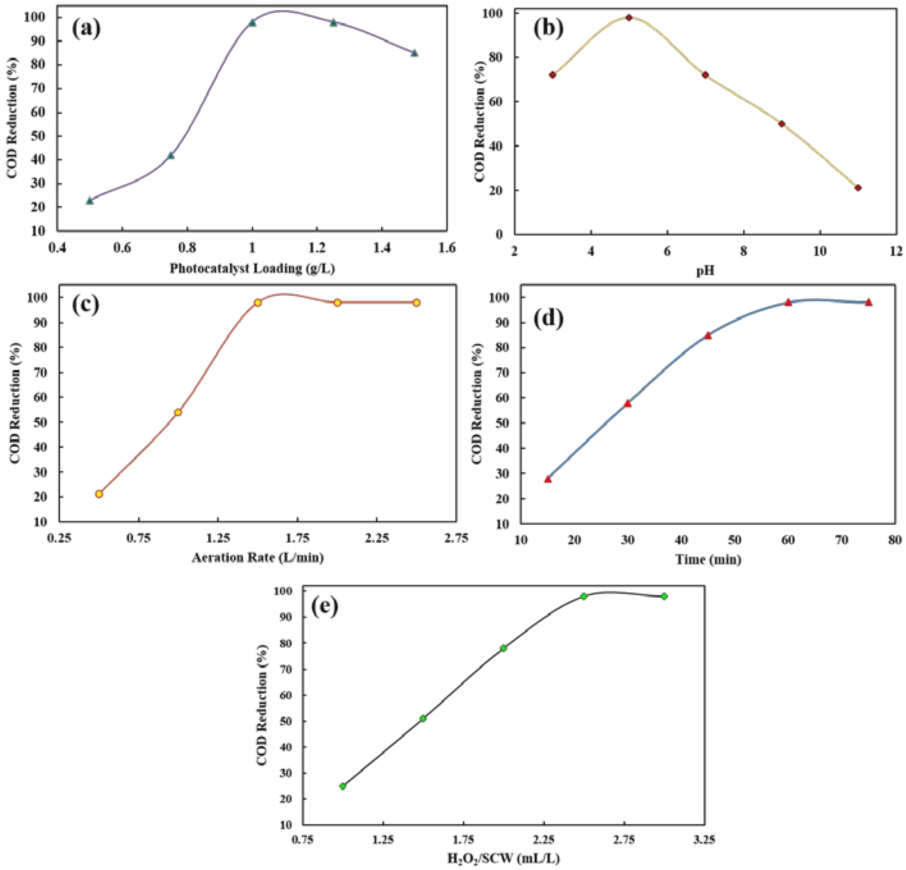

**Fig. 10.** The effects of operational parameters on COD reduction. (a): photocatalyst loading (g/L), (b): pH, (c): Aeration rate (L/min), (d): Time (min), and (e): $H_2O_2$/SCW.

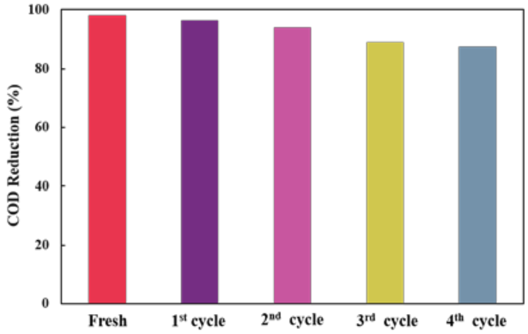

**Fig. 11.** Reusability of the g-$C_3N_4$/$CeFeO_3$ nanocomposites.

### 3.5. *Possible photocatalytic mechanism*

"The interfacial electron transfer in $CeFeO_3$/g-$C_3N_4$ nanocomposites preferentially occurs from g-$C_3N_4$ to $CeFeO_3$, with $CeFeO_3$ serving as the dominant electron-rich site. Upon light irradiation, these $CeFeO_3$/g-$C_3N_4$ nanocomposites facilitate the demineralization of organic pollutants, as depicted in the corresponding Figure 12. Cerium defects located at the interface between g-$C_3N_4$ and $CeFeO_3$ constitute an effective photocatalyst that enhances the spatial separation of photogenerated charges and suppresses interfacial recombination of photoinduced electron-hole pairs."

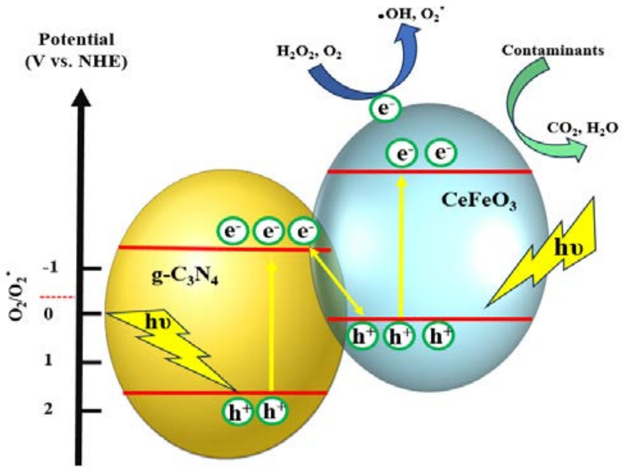

**Fig. 12.** Schematic diagram of photoexcited electron–hole separation process.

### 3.6. *Comparison the performance of $CeFeO_3$/g-$C_3N_4$ NCs with some reported catalysts*

As presented in the Table 3, the performance of the proposed system in COD reduction of spent caustic was benchmarked against existing literature. The results clearly illustrate the proposed system's capability to effectively reduce the COD of spent caustic, requiring only a minimum reaction time.

**Table 3.** Comparison of different catalyst performance for spent caustic wastewater treatment.

| System/Catalyst | Catalyst loading (g/L) | Time (min) | COD Removal (%) |
|---|---|---|---|
| Fenton's process/Ferrous sulfate [46] | 1.0 | 60 | 96.50% |
| Wet air oxidation/Carbonaceous materials [47] | 1.0 | 180 | 60% |
| Wet air oxidation/$FeSO_4$ [48] | 0.80 | 60 | 94% |
| Wet air oxidation /Waste-based carbons [49] | 1.0 | 60 | 60% |
| This work | 1.0 | 60 | 98% |

## 4. Conclusions

This study demonstrated the effectiveness of synthesized g-$C_3N_4$/$CeFeO_3$ nanocomposites as a photocatalyst, achieving 98% COD reduction in petrochemical caustic wastewater under optimized visible light conditions (1.0 g/L catalyst, 2.5 mL/L $H_2O_2$/SCW, pH 5.0, 60 min, 1.5 L/min aeration). The photocatalyst also exhibited promising stability and reusability. Since mass and photon transfer limitations often hinder the scaling up of photocatalytic degradation in conventional reactors, this study evaluated the integration of the developed g-$C_3N_4$/$CeFeO_3$ photocatalyst within advanced reactor designs, such as Taylor-Couette reactors. These reactors offer enhanced mixing and light distribution capabilities, potentially overcoming current limitations and leading to more efficient and industrially relevant wastewater treatment solutions. Investigating this integration represents a crucial next step towards practical implementation.

## Abbreviations

AOPs- Advanced Oxidation Processes
BET- Brunauer Emmett Teller
BOD- Biological Oxygen Demand
COD- Chemical Oxygen Demand
DRS- Diffuse Reflectance Spectroscopy
EDX- Energy Dispersive X-Ray

Fe-MOFs- Iron based MOFs
FE-SEM- Field-Emission Scanning Electron Microscopy
FT-IR- Fourier-Transform Infrared Spectroscopy
MOFs – Metal Organic Frameworks
SCW- Spent Caustic Wastewater
WAO- Wet Air Oxidation
WWTF- Wastewater Treatment Facility
XRD- X-Ray Diffraction

## Acknowledgements

The authors extend their gratitude to the Faculty of Gas and Petroleum at Yasouj University for providing access to laboratory resources.

## References

[1] Tian, X., Song, Y., Shen, Z., Zhou, Y., Wang, K., Jin, X., ... & Liu, T. (2020). A comprehensive review on toxic petrochemical wastewater pretreatment and advanced treatment. Journal of cleaner production, 245, 118692. https://doi.org/10.1016/j.jclepro.2019.118692

[2] Liu, L., Shen, Y., Jiang, X., Zhuang, X., Liu, C., Pan, J., & Liu, F. (2025). Microplastics in petrochemical wastewater: A comprehensive review of removal mechanism, influencing factors and effects on wastewater reuse process. Separation and Purification Technology, 131832. https://doi.org/10.1016/j.seppur.2025.131832

[3] Kondaveeti, S., Govindarajan, D., Mohanakrishna, G., Thatikayala, D., Abu-Reesh, I. M., Min, B., ... & Aminabhavi, T. M. (2023). Sustainable bioelectrochemical systems for bioenergy generation via waste treatment from petroleum industries. Fuel, 331, 125632. https://doi.org/10.1016/j.fuel.2022.125632

[4] Andreides, D., Varga, Z., Pokorna, D., & Zabranska, J. (2021). Performance evaluation of sulfide-based autotrophic denitrification for petrochemical industry wastewater. Journal of Water Process Engineering, 40, 101834. https://doi.org/10.1016/j.jwpe.2020.101834

[5] Wang, K., Chen, X., Yan, D., Xu, Z., Hu, P., & Li, H. (2022). Petrochemical and municipal wastewater treatment plants activated sludge each own distinct core bacteria driven by their specific incoming wastewater. Science of The Total Environment, 826, 153962. https://doi.org/10.1016/j.scitotenv.2022.153962

[6] Gholami, A., Mousavi, S. B., Heris, S. Z., & Mohammadpourfard, M. (2024). Highly efficient treatment of petrochemical spent caustic effluent via electro-Fenton process for COD and TOC removal: optimization and experimental. Biomass Conversion and Biorefinery, 14(15), 17481-17497. https://doi.org/10.1007/s13399-023-03772-2

[7] Natarajan, P., Jayavel, K., Somasundaram, S., & Ganesan, S. (2021). Integrated catalytic oxidation and biological treatment of spent caustic wastewater discharged from petrochemical industries. Energy, Ecology and Environment, 6(2), 160-169. https://doi.org/10.1007/s40974-020-00178-y

[8] Jiang, Y., Li, C., Hou, Z., Shi, X., Zhang, X., Gao, Y., & Deng, S. H. (2023). Pollutants removal and connections among sludge properties, metabolism potential and microbial characteristics in aerobic granular sequencing batch reactor for petrochemical wastewater treatment. Journal of Environmental Management, 344, 118715. https://doi.org/10.1016/j.jenvman.2023.118715

[9] Agarwal, M., & Sudharsan, J. (2021). A comprehensive review on scavenging H2S compounds in oil and gas industry by using nanomaterials. Materials Today: Proceedings, 44, 1504-1510. https://doi.org/10.1016/j.matpr.2020.11.693

[10] Bayout, A., Cammarano, C., Costa, I. M., Veryasov, G., & Hulea, V. (2024). Management of methyl mercaptan contained in waste gases—an overview. Environmental Science and Pollution Research, 31(32), 44669-44690. https://doi.org/10.1007/s11356-024-34112-0

[11] Wang, H., Sun, S., Nie, L., Zhang, Z., Li, W., & Hao, Z. (2023). A review of whole-process control of industrial volatile organic compounds in China. Journal of Environmental Sciences, 123, 127-139. https://doi.org/10.1016/j.jes.2022.02.037

[12] Shokri, A., & Nasernejad, B. (2023). Treatment of spent caustic wastewater by electro-Fenton process: kinetics and cost analysis. Process

Safety and Environmental Protection, 172, 836-845. https://doi.org/10.1016/j.psep.2023.02.077

[13] Ahmadpour, A., Bozorgian, A., Eslamimanesh, A., & Mohammadi, A. H. (2022). Photocatalytic treatment of spontaneous petrochemical effluents by TiO2 CTAB synthetic nanoparticles. Desalination and Water Treatment, 249, 297-308. https://doi.org/10.5004/dwt.2022.28051

[14] Shokri, A., & Fard, M. S. (2023). Kinetic, statistical, and cost evaluations in the remediation of spent caustic wastewater by photo-electro-Fenton process. International Journal of Environmental Science and Technology, 20(10), 11207-11218. https://doi.org/10.1007/s13762-023-05149-4

[15] Bahadoran, A., De Lile, J. R., Masudy-Panah, S., Sadeghi, B., Li, J., Sabzalian, M. H., ... & Gopinathan, A. (2022). Photocatalytic materials obtained from e-waste recycling: Review, techniques, critique, and update. Journal of Manufacturing and Materials Processing, 6(4), 69. https://doi.org/10.3390/jmmp6040069

[16] Zhang, Y., Wang, Y., Xie, R., Huang, H., Leung, M. K., Li, J., & Leung, D. Y. (2022). Photocatalytic oxidation for volatile organic compounds elimination: from fundamental research to practical applications. Environmental Science & Technology, 56(23), 16582-16601. https://doi.org/10.1021/acs.est.2c05444

[17] Elmi, R., Nejaei, A., Farshi, A., Ramazani, M. E., & Alaie, E. (2021). Comparison of two methods of neutralization and wet air oxidation for treating wastewater spent caustic produced by oil refineries. Environmental Monitoring and Assessment, 193, 1-24. https://doi.org/10.1007/s10661-021-09625-7

[18] Tian, X., Rao, F., León-Patiño, C. A., & Song, S. (2021). Co-disposal of MSWI fly ash and spent caustic through alkaline-activation consolidation. Cement and Concrete Composites, 116, 103888. https://doi.org/10.1016/j.cemconcomp.2020.103888

[19] Shokri, A., & Nasernejad, B. (2024). Electrocoagulation process for spent caustic treatment: Optimization, sludge analysis and economic studies. Journal of Industrial and Engineering Chemistry, 135, 471-479. https://doi.org/10.1016/j.jiec.2024.01.058

[20] Hashemi, S. R., Heydarinasab, A., & Amoozegar, M. A. (2020). Modified biological treatment of spent caustic effluent from liquefied petroleum gas plants. Chemical Engineering & Technology, 43(2), 380-385. https://doi.org/10.1002/ceat.201900368

[21] Chen, F., Jiang, F., Zhu, Y., Hua, Z., Wang, L., Ma, J., ... & Tsiakaras, P. (2024). Three-dimensional electro-Fenton system with steel-slag based particle electrode for the treatment of refinery spent caustic. Journal of Environmental Chemical Engineering, 12(2), 112429. https://doi.org/10.1016/j.jece.2024.112429

[22] Fatehbasharzad, P., Aliasghari, S., Bazargan, A., & Moftakhari Anasori Movahed, S. (2021). Removing sulfide from spent caustic petrochemical wastewater with electro-Fenton treatment. Journal of Applied Water Engineering and Research, 9(4), 315-323. https://doi.org/10.1080/23249676.2021.1947401

[23] Wang, H., Li, X., Zhao, X., Li, C., Song, X., Zhang, P., & Huo, P. (2022). A review on heterogeneous photocatalysis for environmental remediation: From semiconductors to modification strategies. Chinese Journal of Catalysis, 43(2), 178-214. https://doi.org/10.1016/S1872-2067(21)63910-4

[24] Li, J., Wang, Q., Liang, J., Li, H., Guo, S., El-Din, M. G., & Chen, C. (2021). An enhanced disintegration using refinery spent caustic for anaerobic digestion of refinery waste activated sludge. Journal of Environmental Management, 284, 112022. https://doi.org/10.1016/j.jenvman.2021.112022

[25] Tong, Y., Wang, X., Zhang, Y., Xu, J., & Sun, C. (2024). Reactive species in peracetic acid-based AOPs: A critical review of their formation mechanisms, identification methods and oxidation performances. Water Research, 122917. https://doi.org/10.1016/j.watres.2024.122917

[26] Koundle, P., Nirmalkar, N., Momotko, M., Makowiec, S., & Boczkaj, G. (2024). Tetracycline degradation for wastewater treatment based on ozone nanobubbles advanced oxidation processes (AOPs)–Focus

on nanobubbles formation, degradation kinetics, mechanism and effects of water composition. Chemical Engineering Journal, 501, 156236. https://doi.org/10.1016/j.cej.2024.156236

[27] Xie, Z. H., He, C. S., Pei, D. N., Dong, Y., Yang, S. R., Xiong, Z., ... & Lai, B. (2023). Review of characteristics, generation pathways and detection methods of singlet oxygen generated in advanced oxidation processes (AOPs). Chemical Engineering Journal, 468, 143778. https://doi.org/10.1016/j.cej.2023.143778

[28] Jabbar, Z. H., & Graimed, B. H. (2022). Recent developments in industrial organic degradation via semiconductor heterojunctions and the parameters affecting the photocatalytic process: A review study. Journal of Water Process Engineering, 47, 102671. https://doi.org/10.1016/j.jwpe.2022.102671

[29] Al-Tameemi, H. M., Sukkar, K. A., Abbar, A. H., & Kuraimid, Z. K. (2024). Optimization of photocatalytic process with SnO2 catalyst for COD reduction from petroleum refinery wastewater using a slurry bubble photoreactor. Case Studies in Chemical and Environmental Engineering, 9, 100687. https://doi.org/10.1016/j.cscee.2024.100687

[30] Jasim, M. A., & AlJaberi, F. Y. (2023). Removal of COD from real oily wastewater by electrocoagulation using a new configuration of electrodes. Environmental Monitoring and Assessment, 195(6), 651. https://doi.org/10.1007/s10661-023-11257-y

[31] Katare, A., & Saha, P. (2024). Efficient removal of COD, BOD, oil & grease, and turbidity from oil-field produced water via electrocoagulation treatment. Environmental Science and Pollution Research, 31(51), 60988-61003. https://doi.org/10.1007/s11356-024-35294-3

[32] Abdelfattah, I., & Ismail, A. A. (2023). Reduction of COD concentration and complete removal of phenol in industrial wastewater utilizing mesoporous TiO2 nanoparticles under UVA illumination. Optical Materials, 145, 114410. https://doi.org/10.1016/j.optmat.2023.114410

[33] Munien, C., Kweinor Tetteh, E., Govender, T., Jairajh, S., Mguni, L. L., & Rathilal, S. (2023). Turbidity and COD removal from municipal wastewater using a TiO2 photocatalyst—a comparative study of UV and visible light. Applied Sciences, 13(8), 4766. https://doi.org/10.3390/app13084766

[34] Fathirad, F. (2023). Ni and Fe mixed oxide anchored on CNTs, GONRs, and Ti3C2 Mxene as efficient nanocatalysts for direct power generation from methanol electro-oxidation. Materials Chemistry and Physics, 305, 127976. https://doi.org/10.1016/j.matchemphys.2023.127976

[35] Karami, M., & Fathirad, F. (2023). Cobalt ferrite nanoparticles anchored on reduced graphene oxide nanoribbons (0D/1D CoFe2O4/rGONRs) as an efficient catalyst for hydrogen generation via NaBH4 hydrolysis. Inorganic Chemistry Communications, 150, 110552. https://doi.org/10.1016/j.inoche.2023.110552

[36] Zhong, K., Wang, Y., Wu, Q., You, H., Zhang, H., Su, M., ... & Tang, J. (2020). Highly conductive skeleton Graphitic-C3N4 assisted Fe-based metal-organic frameworks derived porous bimetallic carbon nanofiber for enhanced oxygen-reduction performance in microbial fuel cells. Journal of Power Sources, 467, 228313. https://doi.org/10.1016/j.jpowsour.2020.228313

[37] Rana, G., Dhiman, P., Kumar, A., Dawi, E. A., & Sharma, G. (2024). Visible-light driven Z-scheme g-C3N4/Fe-MOF photocatalyst for degradation of organic pollutants. Journal of Inorganic and Organometallic Polymers and Materials, 34(6), 2688-2704. https://doi.org/10.1007/s10904-024-03005-7

[38] Fathirad, F., & Sadeghi, E. (2024). NiFe2O4/Ti3C2 nanocomposite as an efficient catalyst for methanol electro-oxidation reaction: investigating annealing temperature and synergetic effect. Fuel, 358, 130130. https://doi.org/10.1016/j.fuel.2023.130130

[39] Afzali, D., Padash, M., Fathirad, F., & Mostafavi, A. (2015). Determination of trace amounts of antimony (III) based on differential pulse voltammetric method with multi-walled

carbon-nanotube-modified carbon paste electrode. Ionics, 21, 565-570. https://doi.org/10.1007/s11581-014-1200-6

[40] Versteyhe, D., Binnemans, K., & Van Gerven, T. (2025). Recent advancements in centrifugal contactor design for chemical processing. Current Opinion in Chemical Engineering, 47, 101084. https://doi.org/10.1016/j.coche.2024.101084

[41] Du, S., Yang, X., Zhu, Y., Yan, S., & Bai, Z. (2025). Visualization investigation of bubble dynamic characteristics for different motion mode in a Taylor-Couette reactor. Chemical Engineering Journal, 160099. https://doi.org/10.1016/j.cej.2025.160099

[42] Schrimpf, M., Esteban, J., Warmeling, H., Färber, T., Behr, A., & Vorholt, A. J. (2021). Taylor-Couette reactor: Principles, design, and applications. AIChE Journal, 67(5), e17228. https://doi.org/10.1002/aic.17228

[43] López-Guajardo, E. A., Galluzzi, R., Delgado-Licona, F., & Morales-Menendez, R. (2024). Process intensification of a catalytic-wall Taylor-Couette reactor through unconventional modulation of its angular speed. Chemical Engineering Journal, 489, 151174. https://doi.org/10.1016/j.cej.2024.151174

[44] Bui, H. K., Nguyen, T. T. H., & Seo, T. S. (2025). Rainbow reactor: Creation of a series of perovskite nanocrystals in a single customizable Couette-Taylor reactor. Chemical Engineering Journal, 161297. https://doi.org/10.1016/j.cej.2025.161297

[45] Wang, C., Yan, W. C., Ran, X., Pu, Z. W., & Shi, W. D. (2024). Experimental and numerical study of photocatalysis in Taylor photoreactors with carbon-quantum-dots/BiOCl as catalysts. Chemical Engineering Science, 294, 120114. https://doi.org/10.1016/j.ces.2024.120114

[46] Hawari, A., Ramadan, H., Abu-Reesh, I., & Ouederni, M. (2015). A comparative study of the treatment of ethylene plant spent caustic by neutralization and classical and advanced oxidation. Journal of environmental management, 151, 105-112. https://doi.org/10.1016/j.jenvman.2014.12.038

[47] Uriarte, S. J., Sanchez-Hornero, M. V., Castillejo, F. M., Castilla, M. I. P., & Hernández, J. A. M. (2024). Carbonaceous materials from a petrol primary oily sludge: Synthesis and catalytic performance in the wet air oxidation of a spent caustic effluent. Journal of Environmental Management, 365, 121606. https://doi.org/10.1016/j.jenvman.2024.121606

[48] Barge, A. S., & Vaidya, P. D. (2020). Kinetics of wet air oxidation of sodium sulfide over heterogeneous iron catalyst. International Journal of Chemical Kinetics, 52(2), 92-98. https://doi.org/10.1002/kin.21333

[49] González, C., Pariente, M. I., Molina, R., Espina, L. G., Masa, M. O., Bernal, V., ... & Martinez, F. (2023). Increasing biodegradability of a real amine-contaminated spent caustic problematic stream through WAO and CWAO oxidation using a high specific surface catalyst from petcoke. Chemical Engineering Journal, 460, 141692. https://doi.org/10.1016/j.cej.2023.141692

**How to cite this paper:**

Mosleh, S., Narimani, M. & Daneshyar, A. (2025). Treatment of the spent caustic wastewater using g-$C_3N_4$/$CeFeO_3$ nanocomposites in a Taylor–Couette photocatalytic reactor. Advances in Environmental Technology, 11(3), 341-356. DOI: 10.22104/aet.2025.7458.2075